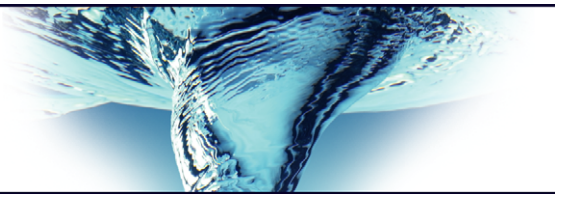
J. Fluid Mech. (2013), *vol.* 736, R2, doi:10.1017/jfm.2013.543



JFM RAPIDS
journals.cambridge.org/rapids

Electrostatically controlled large-amplitude, non-axisymmetric waves in thin film flows down a cylinder

A. W. Wray[1], D. T. Papageorgiou[2] and O. K. Matar[1],†

[1]Department of Chemical Engineering, Imperial College London, South Kensington Campus, London SW7 2AZ, UK

[2]Department of Mathematics, Imperial College London, South Kensington Campus, London SW7 2BZ, UK

(Received 27 June 2013; revised 6 September 2013; accepted 10 October 2013;
first published online 8 November 2013)

We examine the dynamics of a thin film flowing under gravity down the exterior of a vertically aligned inner cylinder, with a co-aligned, concentric cylinder acting as an outer electrode; the space between the outer cylinder and the film is occupied by an inviscid gas. The stability of the interface is studied when it is subjected to an electric field, applied by imposing a potential difference between the two cylinders. Leaky-dielectric theory is used in conjunction with asymptotic reduction, in the large-conductivity limit, to derive a single, two-dimensional evolution equation for the interfacial location, which accounts for gravity, capillarity, and electrostatic effects. A linear stability analysis is carried out which shows that non-axisymmetric modes become more dominant with increasing electric field strength. Our fully two-dimensional numerical solutions of the evolution equation demonstrate qualitative agreement between the trends observed in the nonlinear regime and those predicted by linear theory. These numerical solutions also show that, depending on the electric field strength and the relative proximity of the outer electrode, the interface either remains spatially uniform, or exhibits either axisymmetric or, importantly, non-axisymmetric travelling waves. The effect of wave formation on the interfacial area is investigated in connection with the use of electric fields to control thin film flows to enhance heat and mass transfer rates.

Key words: electrohydrodynamic effects, interfacial flows (free surface), thin films

† Email address for correspondence: o.matar@imperial.ac.uk

© Cambridge University Press 2013

https://doi.org/10.1017/jfm.2013.543 Published online by Cambridge University Press

1. Introduction

A film flowing on the surface of a cylinder is known to experience complex dynamics due to the interaction of a 'Plateau–Rayleigh' instability (Rayleigh 1878) and gravity-induced shear (Frenkel *et al.* 1987). When subjected to electric fields, disparities in the material properties result in Maxwell stresses being induced at the interface in competition with the hydrodynamic mechanisms (Saville 1997). This situation is central to a variety of industrial applications (Darabi, Ohadi & Desiatoun 2000*b*; Darabi, Ohadi & Dessiatoun 2000*a*) but so far has been studied mainly under the assumption of axisymmetry (Wray, Matar & Papageorgiou 2012; Wray, Papageorgiou & Matar 2013); here, this analysis is extended to non-axisymmetric models taking into account azimuthal variation of the film thickness.

We consider a leaky dielectric fluid coating the surface of a vertical cylindrical electrode, surrounded by a gas which is enclosed by a concentric cylinder. We will investigate the nonlinear stability of this system by using long-wave asymptotics to derive a single evolution equation for the film thickness. Low-order modelling of similar systems in the literature has relied predominantly upon one of three asymptotic assumptions. These are based upon considerations of the relative length scales involved in the problem: the radius of the cylinder, the thickness of the liquid layer, the size of the perturbations to the interface, and the characteristic wavelength of the structures involved. Firstly, if the length of the waves is taken to be large relative to the thickness of the fluid, a 'long-wave'-type model results, which has been studied in both the low (Craster & Matar 2006) and moderate (Ruyer-Quil *et al.* 2008) Reynolds number regimes, yielding good agreement with experimental data. However, a necessary assumption appears to be that of axisymmetry, since non-axisymmetric fully nonlinear long waves are not amenable to analysis. Secondly, if the size of the disturbances is taken to be small relative to the thickness of the film, a Kuramoto–Sivashinsky system can arise (Shlang & Sivashinsky 1982). However, this is typically valid only close to threshold. In order to capture non-axisymmetric effects (which are crucial in the presence of electric fields) we consider the third model, where the film thickness is small relative to the radius of the cylinder; this results in a quasi-planar geometry and we show that the equations governing the system are simplified:

$$H_t + \frac{1}{3}(H^3)_z + \boldsymbol{\nabla}\cdot\left(\frac{1}{3}H^3\boldsymbol{\nabla}(H+\nabla^2 H) + \frac{\delta}{2}H^2\boldsymbol{\nabla}H\right) = 0, \tag{1.1}$$

where $\nabla^2 = (\partial_z^2 + \partial_\vartheta^2)$, and H, ϑ, z and t denote the dimensionless film thickness, the azimuthal coordinate, the axial coordinate, and time, respectively, and δ is a dimensionless parameter governing the significance of the electrostatic effects. The second term on the left-hand side is a nonlinear convective term, which may be induced by a concentric flow (Frenkel *et al.* 1987), or indeed by gravity as seen below. The third and fourth terms arise due to capillary forces related to azimuthal and axial curvature gradients. The final term is due to the tangential component of the Maxwell stress. Equation (1.1) was derived in the absence of gravitation and electrostatic effects by Hammond (1983), who studied its one-dimensional form (here we describe a system as one-dimensional if it depends only on the axial variable z and two-dimensional if the interface is non-axisymmetric). It has since been studied extensively in both one- and two-dimensional (Lister *et al.* 2006; Lister, Rallison & Rees 2010) forms. The convective term has been shown (Frenkel *et al.* 1987) to be a nonlinear stabilization term, transferring energy from longer to shorter waves, and staving off thinning.

For the purposes of modelling the electrostatic part of the problem, we use the leaky-dielectric model (Saville 1997), which relies on two assumptions. Firstly, it is

https://doi.org/10.1017/jfm.2013.543 Published online by Cambridge University Press

assumed that both media are finitely conducting, which allows for the accumulation of charge at the interface, resulting in additional stress there, and indeed this coupling arises only at the interface. The second assumption is that the time scale of charge relaxation due to electric conduction is much shorter than that of the flow. This essentially decouples the electrostatic problem from the hydrodynamic one, so that the former may be solved independently given an interfacial configuration. Thus Laplace's equation governs the electrostatic potential in each region, while the problem is closed by the continuity of potential at the interface, Gauss' law, and an interfacial charge evolution equation. This system of equations allows one to model the electrostatically modified gravity-driven flow, which affords a high degree of control over the motion of a fluid; such systems have been the focus of numerous studies, especially in planar (Craster & Matar 2005) and jet-like (Mestel 1996; Gañán-Calvo 1997; Gañán-Calvo & Montanero 2009) geometries. Due to their utility in the contexts of heat and mass transfer (Darabi *et al.* 2000*b*,*a*; Conroy *et al.* 2011), we wish to examine the use of electric fields as a mechanism for controlling coating flows on the exterior of a cylinder.

Previous studies have included nonlinear, one-dimensional versions of both the long-wave (Wray *et al.* 2013) and thin-film (Wray *et al.* 2012) situations, as well as linear studies of the two-dimensional case (Li *et al.* 2009). It is expected that the total free surface area of the system, closely linked to intended goals of the augmentation or suppression of heat and mass transfer, should be dependent upon the electric field applied. However, as yet no nonlinear studies exist in the non-axisymmetric regime, and it is this that we pursue here. As seen previously (Wray *et al.* 2012) the models constructed herein are likely to be stiff, especially for strong electric fields. Therefore, it is beneficial to construct implicit numerical methods. Operator splitting methods have been previously used (Witelski & Bowen 2003; Lister *et al.* 2010) to retain both accuracy and stability without incurring high computational costs. This is the approach we adopt here, which allows us to calculate fully non-axisymmetric interfaces and investigate them parametrically.

We begin by discussing briefly the derivation of the model equation to be used in § 2. We then carry out a linear stability analysis before performing a systematic parametric study involving nonlinear computations, which are discussed in § 3. Our conclusions are given in § 4.

2. Model

We model the flow of a thin film of density ρ and viscosity μ down the exterior surface of a vertical cylinder of radius a under the combined effects of gravity and an applied electric field. The liquid and gas regions have constant conductivities σ_F and σ_A and relative permittivities ϵ_F and ϵ_A respectively. The outer electrode of radius b is held at a constant potential ϕ_b. The disparity in electrical properties between the two regions results in charge accumulation at the interface. Additional stress is exerted which couples into the hydrodynamic problem at the interface via the Maxwell stress tensor (Wray *et al.* 2012). In cylindrical coordinates $(\hat{r}, \vartheta, \hat{z})$ with corresponding velocity field $\hat{\boldsymbol{u}} = (\hat{u}, \hat{v}, \hat{w})$, we non-dimensionalize all variables (carets designate dimensional variables) using

$$\left.\begin{aligned} &\hat{u} = Vu; \quad \hat{v} = Vv; \quad \hat{w} = Vw; \quad \hat{r} = ar; \quad \hat{z} = az; \quad \hat{p} = \frac{V\mu}{a}p; \\ &\hat{t} = \frac{a}{V}t; \quad \hat{q} = \frac{\epsilon_0\phi_b}{a}q; \quad \hat{\phi}^{F,A} = \phi_b\phi^{F,A}, \end{aligned}\right\} \tag{2.1}$$

https://doi.org/10.1017/jfm.2013.543 Published online by Cambridge University Press

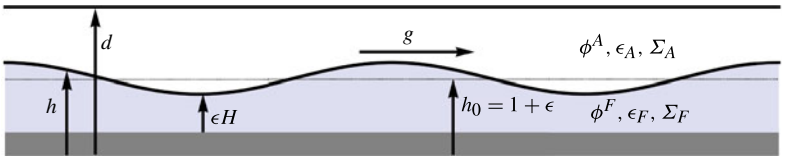


FIGURE 1. Diagram of the situation being studied for $r > 0$: dimensionless film radius h, outer cylinder radius d, scaled basic solution h_0 and thickness ϵH.

where p, q and ϕ denote the pressure, interfacial charge density and voltage potential respectively, the indices A and F refer to the outer hydrodynamically passive and inner film regions, respectively, and ϵ_0 is the permittivity of free space; the characteristic velocity is $V = \rho g a^2/\mu$ in which g is the gravitational acceleration. This scaling gives rise to the dimensionless groups

$$Re = \frac{\rho V a}{\mu}; \quad Ca = \frac{V\mu}{\gamma}; \quad d = \frac{b}{a}; \quad E_b = \frac{\epsilon_0 \phi_b^2}{\mu V}; \quad \Sigma_i = \frac{\sigma_i/\epsilon_0}{a/V}, \quad i = F, A, \tag{2.2}$$

which correspond to a Reynolds number, capillary number, dimensionless position of the outer cylinder, an electrostatic capillary number, and the dimensionless conductivities of the liquid and gas regions, respectively; here γ is the (constant) surface tension.

There exists an exact Nusselt-like solution with a perfectly cylindrical interface at $r = h_0 = \text{const.}$, $\boldsymbol{u} = (0, 0, \bar{w}(r))$ and $\phi^{F,A} = \bar{\phi}^{F,A}(r)$, where

$$\left.\begin{aligned} &\bar{w} = -\frac{1}{4}[r^2 - 1 - 2h_0^2 \log(r)]; \quad \bar{\phi}^F = \frac{\log r}{\log(h_0) - \sigma_R \log(h_0/d)}; \\ &\bar{\phi}^A = \frac{\sigma_R \log(r/h_0) + \log(h_0)}{\log(h_0) - \sigma_R \log(h_0/d)}, \end{aligned}\right\} \tag{2.3}$$

where $\sigma_R = \sigma_F/\sigma_A$ is the ratio of the conductivities in the two regions.

In order to make analytical progress on a nonlinear evolution equation, the small value of the film thickness to cylinder radius ratio is exploited, so that $h_0 = 1 + \epsilon$. Expanding the base states asymptotically, we seek appropriate scalings when the radial coordinate inside the liquid layer is $r = 1 + \epsilon R$, with the interface at $r = 1 + \epsilon H$. Allowing the Reynolds number to be very small so that inertial effects may be neglected, and scaling $Ca = \epsilon \widetilde{Ca}$ to promote surface tension effects, with $\widetilde{Ca} = O(1)$, this leads to

$$w = \epsilon^2 w_0 + \cdots, \quad u = \epsilon^3 u_0 + \cdots, \quad v = \epsilon^2 v_0 + \cdots, \quad p = p_0 + \cdots. \tag{2.4}$$

Note that no such asymptotic scaling is made on the radius of the outer electrode d. A schematic is given in figure 1. The governing equations for the hydrodynamic part of the problem are the scaled Navier–Stokes equations at leading order:

$$p_{0R} = 0, \quad v_{0RR} = p_{0\vartheta}, \quad w_{0RR} = (p_{0z} - 1), \quad u_{0R} + v_{0\vartheta} + w_{0z} = 0, \tag{2.5}$$

together with the interfacial stress conditions at $R = H$,

$$v_{0R} = E^{\vartheta}(z, \vartheta), \quad w_{0R} = E^{z}(z, \vartheta), \quad p_0 = \frac{1}{\widetilde{Ca}}\left[\frac{1}{\epsilon} - (H + \nabla^2 H)\right] + E^{N}(z, \vartheta), \tag{2.6}$$

where E^{ϑ}, E^{z} and E^{N} are the azimuthal, axial and normal contributions of the electric stress at the interface, given explicitly shortly. Using a slow time $t = \tilde{t}/\epsilon^2$ to capture

https://doi.org/10.1017/jfm.2013.543 Published online by Cambridge University Press

the dynamics, and dropping the tilde decoration, the kinematic condition is, to leading order,

$$H_t = u_0 - v_0 H_\vartheta - w_0 H_z = -\begin{pmatrix}\partial_\vartheta \\ \partial_z\end{pmatrix} \cdot \int_0^H \begin{pmatrix} v_0 \\ w_0 \end{pmatrix} \mathrm{d}R. \tag{2.7}$$

Solving (2.5) for the leading-order axial and azimuthal velocity components gives

$$w_0 = (p_{0_z} - 1)\left(\frac{R^2}{2} - HR\right) + E^z R, \quad v_0 = p_{0\vartheta}\left(\frac{R^2}{2} - HR\right) + E^\vartheta R. \tag{2.8}$$

To solve the electrostatic part of the perturbed problem we pose

$$\phi^F = \epsilon\phi_0^F(R, \vartheta,) + \epsilon^2\phi_1^F(R, \vartheta, z) + \cdots, \quad \phi^A = \phi_0^A(r, \vartheta, z) + \epsilon\phi_1^A(r, \vartheta, z,) + \cdots. \tag{2.9}$$

Application of the chain rule to the Laplace equation governing ϕ^F gives $\phi^F_{0\,RR} + \epsilon(\phi^F_{0\,R} + \phi^F_{1\,RR}) + \cdots = 0$. Taking the conductivities to be large ($\Sigma_{F,A} \gg 1$) induces continuity of current at the interface (Wray *et al.* 2012) giving $\sigma_R \nabla\phi^F \cdot \boldsymbol{n} = \nabla\phi^A \cdot \boldsymbol{n}$. Thus in scaled variables,

$$\sigma_R \phi^F_{0R}|_{R=H} + O(\epsilon) = (\phi^A_{0r} - h^{-2}h_\vartheta \phi^A_{0\vartheta} - h_z\phi^A_{0z})|_{r=1} + O(\epsilon), \tag{2.10}$$

where the right-hand side has been expanded about $r = 1$. The fields are also continuous at the interface so that $\phi^F|_{R=H} = \phi^A|_{r=h} \Rightarrow \phi^A_0|_{r=1} = 0 + O(\epsilon)$.

We may now solve order by order: $\nabla^2\phi^A_0 = 0$ is solved subject to equipotential at the outer electrode, $\phi^A_0|_{r=d} = 1$, and $\phi^A_0|_{r=1} = 0$; $\phi^F_{0\,RR} = 0$ is then solved subject to equipotential at the inner electrode, $\phi^F|_{R=0} = 0$ and (2.10), giving respectively,

$$\phi^A_0 = \frac{\log r}{\log d}, \quad \phi^F_0 = \frac{R}{\sigma_R \log d}. \tag{2.11}$$

These solutions $\phi^F_0(R)$ and $\phi^A_0(r)$ are in fact the leading-order expansions of the basic solutions (2.3). This is sufficient to determine the requisite electrostatic terms in (2.6) to leading order:

$$E^N_z = \frac{E_b}{2}(\epsilon_A {\phi^A_{0r}}^2 - \epsilon_F {\phi^F_{0R}}^2)_z = 0, \tag{2.12}$$

$$E^z = E_b(\epsilon_A\phi^A_{0r} - \epsilon_F\phi^F_{0R})(\phi^F_{0R}H_z) = \delta H_z, \tag{2.13}$$

$$E^\vartheta = E_b(\epsilon_A\phi^A_{0r} - \epsilon_F\phi^F_{0R})(\phi^F_{0R}H_\vartheta) = \delta H_\vartheta. \tag{2.14}$$

Note that $\delta = E_b/(\sigma_R(\log d)^2)(\epsilon_A - \epsilon_F/\sigma_R)$ may be either positive or negative, and governs the relative significance of the interfacial tangential stress induced by the electric fields. Substitution of (2.12) into (2.6), as well as (2.13) and (2.14) into (2.8), and the latter into (2.7) gives

$$H_t + \frac{1}{3}(H^3)_z + \nabla \cdot \left(\frac{1}{3\widetilde{Ca}}H^3\nabla(H + \nabla^2 H) + \frac{\delta}{2}H^2\nabla H\right) = 0. \tag{2.15}$$

This is the evolution equation that we shall analyse in the remainder of the paper. We note that the role of $\widetilde{Ca}$ is well understood having been studied extensively elsewhere (Kerchman & Frenkel 1994) and so for the purposes of this paper we take the canonical limit $\widetilde{Ca} = 1$. The results we present are expected to extend naturally for other values of $\widetilde{Ca}$ and indeed this has been the case in additional representative

https://doi.org/10.1017/jfm.2013.543 Published online by Cambridge University Press

calculations which we have performed. Note also that this equation is a generalization of several existing equations in the literature. If axisymmetry is assumed, this equation becomes $H_t + (H^3)_z/3 + \partial_z(H^3/3(H_z + H_{zzz}) + (\delta/2)H^2 H_z) = 0$, as studied by Wray *et al.* (2012). For $\delta = 0$, the equation of Frenkel *et al.* (1987) is recovered. If both $\delta = 0$ and the gravitational term $(H^3)_z/3$ are removed, the equations studied by Hammond (1983) and Lister *et al.* (2010) are recovered.

3. Results

Equation (2.15) is linearized using normal modes, $H - 1 \sim \mathrm{e}^{\mathrm{i}(kz+n\vartheta)}\mathrm{e}^{\sigma t}$, to give

$$\sigma + \mathrm{i}k - \frac{1}{3}(k^2 + n^2)\left[\left(1 + \frac{3\delta}{2}\right) - (n^2 + k^2)\right] = 0, \tag{3.1}$$

where σ is the (complex) temporal growth rate, and k and n are the (real) disturbance wavenumbers in the axial and azimuthal directions, respectively. It is noted that n may only take integer values. The wavenumbers associated with the cutoff, k_c, and most dangerous mode, k_{max}, are given by

$$k_c = (1 + \tfrac{3}{2}\delta - n^2)^{1/2}, \quad k_{max} = (\tfrac{1}{2} + \tfrac{3}{4}\delta - n^2)^{1/2}. \tag{3.2}$$

In the electrically passive case, $\delta = 0$, it is seen that only the $k_c = 0$, axially uniform, non-axisymmetric mode is supported. This is due to the assumptions that the film is thin relative to the radius of the cylinder, and that the capillary number is small, and is in line with the results of Frenkel *et al.* (1987). This is of course in contrast to the planar case where spanwise instabilities exist in the absence of electric fields; a limit which can be recovered in other cylindrical regimes (Shlang & Sivashinsky 1982; Kalliadasis & Chang 1994; Ruyer-Quil *et al.* 2008). For $\delta > 0$, k_c is strictly positive for $1 + 3\delta/2 > n^2$ so that higher non-axisymmetric modes ($n \geqslant 1$) can be supported. Figure 2 shows the dependence of k_c on δ with n varying incrementally. Inspection of this figure reveals that increasing δ leads to an increase in k_c, and is thus destabilizing. It is also seen that for fixed k_c, increasing δ promotes the formation of non-axisymmetric modes of higher n. This is because increasing δ constitutes imposing a destabilizing interfacial isotropic shear stress due to the variation in electric fields across the interface. We turn to the nonlinear two-dimensional simulations next.

In order to solve (2.15) numerically we have developed two schemes similar to those of Witelski & Bowen (2003). One scheme is semi-implicit, first-order in time and second-order in space, discretized using finite differences. The second scheme is second-order in time and pseudospectral in space: differentiations are conducted in Fourier space while multiplications are calculated in real space. The latter is given by

$$\left(I + \tfrac{2}{3}\Delta t(D_x^2 + D_x^4)\right)\Delta u_{(k),int}^{n+1} = -\tfrac{1}{3}(3\tilde{u}_{(k)}^{n+1} - 4u^n + u^{n-1}) - \tfrac{2}{3}\Delta t\nabla\cdot(f\nabla\tilde{u}_{(k)}^{n+1} + g\nabla^3\tilde{u}_{(k)}^{n+1}) - \tfrac{1}{3}\partial_x(\tilde{u}_{(k)}^{n+1^3}), \tag{3.3}$$

$$\left(I + \tfrac{2}{3}\Delta t(D_y^2 + D_y^4)\right)\Delta u_{(k)}^{n+1} = \Delta u_{(k),int}^{n+1}, \tag{3.4}$$

$$\tilde{u}_{(k+1)}^{n+1} = \tilde{u}_{(k)}^{n+1} + \Delta u_{(k)}^{n+1}, \tag{3.5}$$

where Δt is the time step, I is the identity operator and the iteration is initially seeded with $\tilde{u}_{(0)}^{n+1} = 2u^n - u^{n-1}$; $D_{x,y}^2 = f(\tilde{u}^{n+1})\partial_{x,y}^{(2)}$; $D_{x,y}^4 = g(\tilde{u}^{n+1})\partial_{x,y}^{(4)}$; $f(H) = (H^3/3 + \delta(H^2/2))$; and $g(H) = H^3/3$, so that u^n (not to be confused with the radial velocity component) is the discrete approximation to the interfacial shape H at $t = t_n$. This more accurate but

https://doi.org/10.1017/jfm.2013.543 Published online by Cambridge University Press

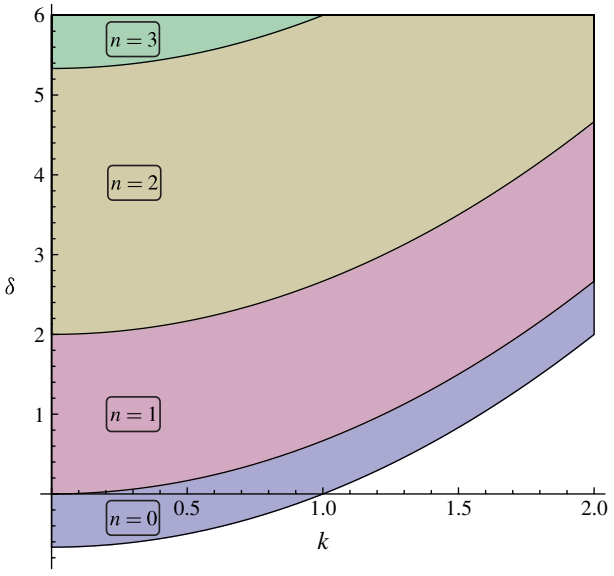


FIGURE 2. Neutral stability curves in the k–δ plane for different n values, where k and n are the axial and azimuthal wavenumbers respectively, and δ is a dimensionless parameter governing the significance of the electrostatic contribution to tangential stress at the interface.

more computationally intensive scheme has been used to validate the accuracy of the first-order scheme. The latter has been used for the majority of the computations given herein. Additional validations have been made of the first-order scheme against one-dimensional computations (performed using an existing one-dimensional code, second-order in time and pseudospectral in space, as used in Wray *et al.* 2013) and the linear theory discussed above. In all cases, agreement has been excellent. Convergence has been checked by verifying that identical results are obtained upon mesh refinement.

A parametric study has been performed for $-1 \leqslant \delta \leqslant 2.5$ on a periodic domain with $(z, \vartheta) \in [0, 30) \times [0, 2\pi)$. The simulations are initially seeded with random noise on H in their spectrum. Computations have been repeated multiple times for different random initial values to ensure validity. Our interest is now two-fold: firstly, to explore the non-axisymmetric structures which are expected for $\delta > 0$; secondly, we are interested in the augmentation or suppression of heat and mass transfer, particularly via the effect of the value of δ on the total free interfacial area.

At each time step, the energy norm $\|H\|_2^2 = \int\int H^2 \,\mathrm{d}\vartheta \,\mathrm{d}z$, the interfacial area and the Fourier spectrum are computed. In all computations, either an axisymmetric perfectly cylindrical state or non-uniform travelling waves are found to emerge, with both cases determined by the emergence of a constant value of $\|H\|_2$. Generically, the system has been found to settle down to the following attractors: (i) a flat state ($\delta < -2/3$); (ii) axisymmetric travelling waves ($-2/3 < \delta \leqslant 0$) such as the double-/triple-crest solutions given in figure 3; or (iii) non-axisymmetric travelling waves ($\delta > 0$) such as the single-/double-drop solutions given in figures 4, 5 and 3. In all cases, travelling waves eventually propagate in a purely axial direction. Note that cases (i) and (ii) are in line with linear theory predictions and have been observed previously in axisymmetric studies (Wray *et al.* 2012).

In order to analyse the nonlinear behaviour of the system, and to examine the degree of non-axisymmetry exhibited by the structures that arise, we need an appropriate

https://doi.org/10.1017/jfm.2013.543 Published online by Cambridge University Press

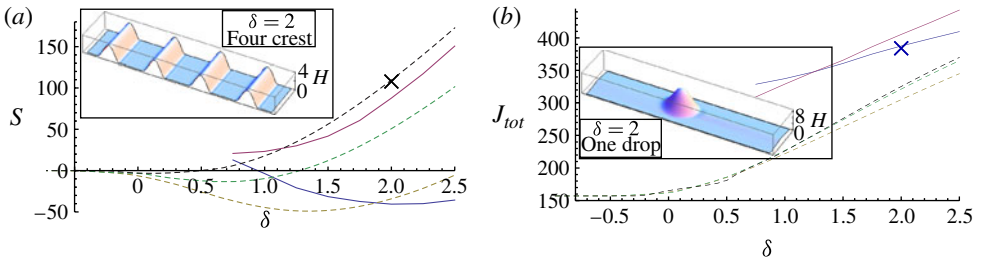


FIGURE 3. (*a*) Increase in free surface area S. (*b*) Total flux J_{tot} for $\Theta = 1$, $K = 0.2$. Dashed lines correspond, bottom to top, to double- (dark yellow), triple- (green) and quadruple-crest (black) one-dimensional solutions. Solid lines, bottom to top by end point, correspond to single- (blue) and double-drop (purple) solutions. Insets correspond to the crosses on the respective branches.

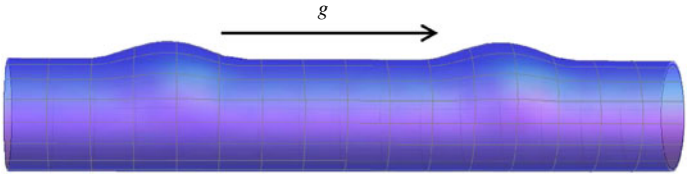


FIGURE 4. A two-drop travelling wave for $\delta = 2.5$.

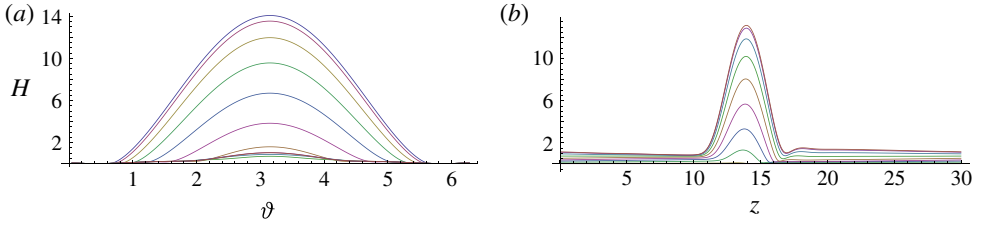


FIGURE 5. Slices through the single-drop configuration depicted in the inset of figure 3(*a*): (*a*) transverse slices for $z = 13.96, 14.46, \ldots, 17.96$; (*b*) streamwise slices for $\vartheta = 0, \pi/10, \ldots, \pi$.

metric. Thus we consider the energy distribution amongst the modes of the Fourier spectrum of the structures formed (in a similar manner to Scheid, Ruyer-Quil & Manneville 2006). In particular, by analogy with linear theory, we consider a 'nonlinear cutoff wavenumber' $k_c(\delta, n)$ defined as follows. At a late time where the system is a nonlinear travelling wave, we define

$$E_{max} := \max_{k,n} |\hat{h}_{k,n}| = |\hat{h}_{k_0,n_0}|, \tag{3.6}$$

where $\hat{h}_{k,n}$ are the values of the discrete Fourier modes corresponding to the shape of the interface, i.e. $H(z, \vartheta, t) = \sum\sum_{k,n} \hat{h}_{k,n}(t) \mathrm{e}^{\mathrm{i}kz} \mathrm{e}^{\mathrm{i}n\vartheta}$. Then for a given n and δ, k_c is the greatest k for which the associated mode exceeds 5 % of this value:

$$k_c(\delta, n) = \max_{|\hat{h}_k| > E_{max}/20} k, \tag{3.7}$$

https://doi.org/10.1017/jfm.2013.543 Published online by Cambridge University Press

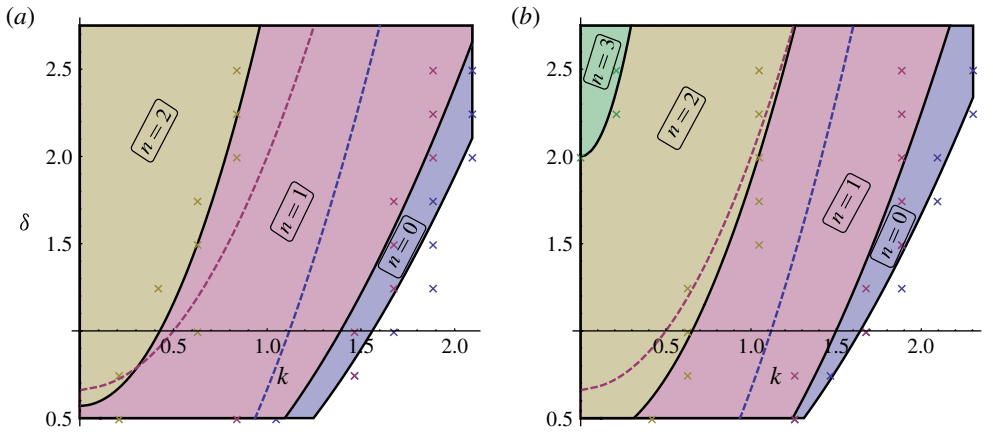


FIGURE 6. Energy distribution comparison between linear and nonlinear modes. (*a*) Single-drop configuration (see figures 3 and 5), (*b*) two drops (see figure 4). Crosses correspond to nonlinear cutoff wavenumbers as prescribed in (3.7), with shaded regions fitted to these points to indicate regions of instability. Dashed lines correspond to the most unstable wavenumbers as predicted by linear theory.

so that for a given azimuthal wavenumber n, k_c is the last axisymmetric wavenumber k with 'significant' energy. This is independent of t once a travelling wave state has been reached. For successive azimuthal wavenumbers n, these values of k_c are plotted in figure 6 as crosses. Note that k_c can only take discrete values as we are solving on a finite periodic domain. By analogy with the characteristic polynomials in (3.2), least-squares fitting is then used on the two-parameter parabola $a_0 + a_2k^2$ to infer the appropriate smooth dependence of k_c on n and δ. The appropriate regions are then shaded and labelled to indicate the nonlinearly unstable modes. The dashed lines are the fastest growing modes as predicted by linear theory. It can be seen that the linear predictions are qualitatively preserved into the nonlinear regime, giving rise to increasingly non-axisymmetric disturbances as the value of δ is increased. Due to nonlinear effects, higher modes are destabilized faster than predicted by linear theory. This results in more complex shapes, potentially giving rise to higher surface area.

An example of a two-drop travelling wave is given in figure 4 for $\delta = 2.5$. To examine the drops that arise in more detail, we give slices through a single drop in figure 5. It is observed from the cross-stream slices that the drops are symmetric about their highest point, exhibiting thinning at the antipodal point of the surface of the cylinder. The streamwise slices exhibit profiles similar to those found in the one-dimensional case, including the presence of preceding capillary ripples.

We also find that there is a strong dependence of free surface area on the value of δ, where the surface area A is given by

$$\begin{aligned} A &= \iint \left[1 + \frac{h_\vartheta^2}{h^2} + h_z^2\right]^{1/2} h \,\mathrm{d}\vartheta \,\mathrm{d}z \\ &= 2\pi L\left(1 + \epsilon + \frac{\epsilon^2}{2}\right) + \frac{\epsilon^2}{2}\iint H_z^2 + H_\vartheta^2 - H^2 \,\mathrm{d}z\,\mathrm{d}\vartheta + O(\epsilon^3), \end{aligned} \tag{3.8}$$

where $L = 30$ is the length of the domain. The variation in the free surface area relative to the undisturbed state is thus given by $\epsilon^2 S/2$ where $S = \iint 1 + H_z^2 + H_\vartheta^2 - H^2 \,\mathrm{d}z\,\mathrm{d}\vartheta$.

https://doi.org/10.1017/jfm.2013.543 Published online by Cambridge University Press

We also consider the instantaneous thermal flux J that would be exhibited by these travelling waves if the inner cylinder were heated. Following Burelbach, Bankoff & Davis (1988), the conduction-dominated temperature field T satisfies $T_{RR} = 0$ at leading order, subject to an energy balance $J = -T_R$, and the wall condition $T = \Theta$, where Θ is a dimensionless quantity representing the departure of the wall temperature from the equilibrium saturation temperature. The problem is closed by a constitutive condition, $T|_{R=H} = KJ$ where K measures the degree of non-equilibrium at the interface. Upon solving these equations, we find that $T = \Theta - JR$, so that $J = \Theta/(K + H)$. The total flux J_{tot} is thus

$$J_{tot} = \iint J\left[1 + \frac{h_\vartheta^2}{h^2} + h_z^2\right]^{1/2} h \,\mathrm{d}\vartheta \,\mathrm{d}z = 2\pi L\Theta \iint \frac{1}{K+H}\,\mathrm{d}z\,\mathrm{d}\vartheta + O(\epsilon). \tag{3.9}$$

The values of S and J_{tot} produced are plotted in figure 3. The results of one-dimensional simulations, which are unstable to spanwise perturbations for $\delta > 0$, are plotted as dashed lines, while the results of two-dimensional simulations are plotted as solid lines. It is observed that for intermediate values of δ surface area may be reduced. However, for higher values of δ, and especially for configurations with more droplets/crests (which will naturally be favoured by higher values of δ), an increase in surface area is observed. It is also seen that increasing δ increases the value of J_{tot}, as the electric field drives the film to drainage resulting in larger thin regions, allowing greater thermal flux.

4. Conclusions

We have used asymptotic reductions and leaky-dielectric theory to derive a single evolution equation for the thickness of a film flowing down the exterior of a vertical cylinder with a concentric cylinder serving as an outer electrode. The introduction of electric fields through a potential difference between the electrodes induces coarsening into non-axisymmetric disturbances. These typically take the form of 'drops' as seen in figure 4. We have thus demonstrated that the common assumption of axisymmetry is not necessarily valid when additional physical effects are incorporated.

We have shown the nonlinear dependence of the shape of the interface on the value of $\delta = E_b/(\sigma_R(\log d)^2)(\epsilon_A - \epsilon_F/\sigma_R)$, demonstrating that although linear theory is indicative of the behaviours that might occur, the full picture is only given by full numerical computations. We have also shown that the system generically exhibits travelling waves. The interfacial area and the thermal flux associated with interfacial heat are critically dependent on the value of δ. This dependence has been studied parametrically and compared to the more limited predictions given by linear theory and one-dimensional calculations. We note that the interfacial area can be increased for sufficiently large values of δ, whereas the thermal flux increases monotonically with δ. This study has demonstrated the potential for using electric fields to control the behaviour of interfacial flows, and the intensification of associated transport rates.

References

Burelbach, J. P., Bankoff, S. G. & Davis, S. H. 1988 Nonlinear stability of evaporating/condensing liquid films. *J. Fluid Mech.* **195**, 463–494.

Conroy, D. T., Matar, O. K., Craster, R. V. & Papageorgiou, D. T. 2011 Breakup of an electrified viscous thread with charged surfactants. *Phys. Fluids* **23** (2), 022103.

https://doi.org/10.1017/jfm.2013.543 Published online by Cambridge University Press

CRASTER, R. V. & MATAR, O. K. 2005 Electrically induced pattern formation in thin leaky dielectric films. *Phys. Fluids* **17**, 032104.

CRASTER, R. V. & MATAR, O. K. 2006 On viscous beads flowing down a vertical fibre. *J. Fluid Mech.* **553**, 85–106.

DARABI, J., OHADI, M. M. & DESSIATOUN, S. V. 2000*a* Augmentation of thin falling-film evaporation on horizontal tubes using an applied electric field. *Trans. ASME: J. Heat Transfer* **122** (2), 391–398.

DARABI, J., OHADI, M. M. & DESIATOUN, S. V. 2000*b* Falling film and spray evaporation enhancement using an applied electric field. *Trans. ASME: J. Heat Transfer* **122** (4), 741–748.

FRENKEL, A. L., BABCHIN, A. J., LEVICH, B. G., SHLANG, T. & SIVASHINSKY, G. I. 1987 Annular flows can keep unstable films from breakup: nonlinear saturation of capillary instability. *J. Colloid Interface Sci.* **115** (1), 225–233.

GAÑÁN-CALVO, A. M. 1997 Cone-jet analytical extension of Taylor's electrostatic solution and the asymptotic universal scaling laws in electrospraying. *Phys. Rev. Lett.* **79** (2), 217–220.

GAÑÁN-CALVO, A. M. & MONTANERO, J. M. 2009 Revision of capillary cone-jet physics: electrospray and flow focusing. *Phys. Rev.* E **79** (6), 066305.

HAMMOND, P. S. 1983 Nonlinear adjustment of a thin annular film of viscous fluid surrounding a thread of another within a circular cylindrical pipe. *J. Fluid Mech.* **137**, 363–384.

KALLIADASIS, S. & CHANG, H.-C. 1994 Drop formation during coating of vertical fibres. *J. Fluid Mech.* **261**, 135–168.

KERCHMAN, V. I. & FRENKEL, A. L. 1994 Interactions of coherent structures in a film flow: simulations of a highly nonlinear evolution equation. *Theor. Comput. Fluid Dyn.* **6** (4), 235–254.

LI, B., LI, Y., XU, G.-K. & FENG, X.-Q. 2009 Surface patterning of soft polymer film-coated cylinders via an electric field. *J. Phys.: Condens. Matter* **21** (44), 445006.

LISTER, J. R., RALLISON, J. M., KING, A. A., CUMMINGS, L. J. & JENSEN, O. E. 2006 Capillary drainage of an annular film: the dynamics of collars and lobes. *J. Fluid Mech.* **552**, 311–344.

LISTER, J. R., RALLISON, M. & REES, S. J. 2010 The nonlinear dynamics of pendent drops on a thin film coating the underside of a ceiling. *J. Fluid Mech.* **647**, 239–264.

MESTEL, A. J. 1996 Electrohydrodynamic stability of a highly viscous jet. *J. Fluid Mech.* **312**, 311–326.

RAYLEIGH, LORD 1878 On the instability of jets. *Proc. R. Soc. Lond.* A **10**, 4–13.

RUYER-QUIL, C., TREVELEYAN, P., GIORGIUTTI-DAUPHIN, F., DUPRAT, C. & KALLIADASIS, S. 2008 Modelling film flows down a fibre. *J. Fluid Mech.* **603**, 431–462.

SAVILLE, D. A. 1997 Electrohydrodynamics: the Taylor–Melcher leaky dielectric model. *Annu. Rev. Fluid Mech.* **29**, 27–64.

SCHEID, B., RUYER-QUIL, C. & MANNEVILLE, P. 2006 Wave patterns in film flows: modelling and three-dimensional waves. *J. Fluid Mech.* **562**, 183–222.

SHLANG, T. & SIVASHINSKY, G. I. 1982 Irregular flow of a liquid film down a vertical column. *J. Phys.* **43** (3), 459–466.

WITELSKI, T. P. & BOWEN, M. 2003 ADI schemes for higher-order nonlinear diffusion equations. *Appl. Numer Maths* **45** (2), 331–351.

WRAY, A. W., MATAR, O. & PAPAGEORGIOU, D. T. 2012 Non-linear waves in electrified viscous film flow down a vertical cylinder. *IMA J. Appl. Maths* **77** (3), 430–440.

WRAY, A. W., PAPAGEORGIOU, D. T. & MATAR, O. K. Electrified coating flows on vertical fibres: enhancement or suppression of interfacial dynamics. *J. Fluid Mech.* **735**, 427–456.

https://doi.org/10.1017/jfm.2013.543 Published online by Cambridge University Press